Article:
Vajpayee, V. orcid.org/0000-0003-1179-7118, Becerra, V., Bausch, N. et al. (3 more authors) (2021) Robust-optimal integrated control design technique for a pressurized water-type nuclear power plant. Progress in Nuclear Energy, 131. 103575. ISSN 0149-1970

https://doi.org/10.1016/j.pnucene.2020.103575

Robust-Optimal Integrated Control Design Technique for a Pressurized Water-type Nuclear Power Plant

Vineet Vajpayee*, Victor Becerra, Nils Bausch, Jiamei Deng, S. R. Shimjith, A. John Arul

***Abstract*—A control design scheme is formulated for a pressurized water type nuclear power plant by integrating the optimal linear quadratic Gaussian (LQG) control with the robust integral sliding mode (ISM) technique. A novel robust-optimal hybrid control scheme is further proposed by integrating the LQG-ISM technique with the loop transfer recovery approach to enhance the effectiveness and robustness capability. The control architecture offers robust performance with minimum control efforts and tracks the reference set-point effectively in the presence of disturbances and parametric uncertainties. The multi-input-multi-output nuclear power plant model adopted in this work is characterized by 38 state variables. The nonlinear plant model is linearized around steady-state operating conditions to obtain a linear model for the controller design. The efficacy of the proposed controllers is demonstrated by nuclear power plant subsystem simulations. The control performance of the proposed technique is also compared with other classical control design schemes. Numerical measures are employed to quantitatively analyse and compare the performance of the different controllers that are studied in the work.**

***Index Terms*—Optimal Control, Robust Control, Sliding Mode, Pressurized Water Reactor, Nuclear Power Plant.**

I. Introduction

Nuclear power plants (NPPs) are complex non-linear systems. Control of NPPs poses challenges due to parameter variations caused by fuel burn-up, internal reactivity feedbacks, modelling uncertainties, and unknown disturbances. System parameters associated with the reactor core, thermal-hydraulics, reactivity feedbacks, etc., differ significantly with operating conditions. The routine load cycles over a broad range of power variations can significantly affect plant performance. Uncertainties in the actuator signals and noisy sensor measurements add further complexities to the control design problem. Consequently, traditional controllers often fail to deliver desirable performance. The plant control systems must be able to respond promptly and safely to fast variations in demand in an uncertain environment. Thus, it is essential to develop improved control techniques which can provide closed-loop stability and enhance the safety and operability of NPPs.

A considerable amount of research has been undertaken in the application of robust control techniques in nuclear reactors, especially for the core power control. In the last two decades, various control design techniques such as state feedback assisted control (SFAC) [1]–[5], $\mathcal{H}_\infty$ control [6]–[9], model predictive control (MPC) [10]–[14], sliding mode control (SMC) [15]–[22], and soft-computing based controls [23]–[26] have been proposed to deal with disturbances and uncertainties in NPPs. Edwards et al. [1] proposed the idea of SFAC to enhance the stability of the classical control loop by integrating a state-feedback compensating loop. The loop transfer recovery (LTR) technique has been combined with linear quadratic Gaussian (LQG) control in an SFAC framework to improve the reactor temperature and power controls during the variation in reactor parameters [2]–[5]. $\mathcal{H}_\infty$-based control schemes have been designed for reactor power control and to obtain enhanced robustness over the classical LQG control scheme [6]–[9]. To deal with system design constraints in an uncertain NPP system, receding horizon-based robust MPC approaches, which solve an optimization problem at each sampling instant, have been proposed [10]–[14].

SMC is another robust control design technique that has been applied to study the load-following problem of nuclear reactors. SMC guarantees robustness to the uncertainties entering through the input channel, once the system reaches the sliding surface [15]–[19]. However, the implementation of SMC is sensitive to uncertainties during the reaching phase. It may also need further control efforts to keep the system on the sliding surface. An integral sliding mode (ISM) control approach has been proposed to avoid these issues in the literature which forces the system trajectories to lie on the sliding surface from the very beginning, thereby avoiding the reaching phase [27]. Hence, robustness is guaranteed throughout the system response. Besides, ISM can be integrated with any existing state-feedback control technique, which makes it very useful for complex systems such as nuclear power plants [20]–[22]. To deal with modelling uncertainties and disturbances, soft-computing techniques have been further incorporated in the controller design. Neural network controllers [23], emotional controllers [24], fuzzy logic controllers [25], and genetic algorithms optimized controllers [26] have been proposed to enhance the capabilities of the classical controllers.

* Corresponding author.

Vineet Vajpayee (vineet.vajpayee@port.ac.uk), Victor Becerra (victor.becerra@port.ac.uk), and Nils Bausch (nils.bausch@port.ac.uk) are with School of Energy and Electronic Engineering, University of Portsmouth, Portsmouth, PO1 3DJ, United Kingdom.

Jiamei Deng (j.deng@leedsbeckett.ac.uk) is with School of Built Environment, Engineering, and Computing, Leeds Beckett University, Leeds, LS6 3QS, United Kingdom.

S. R. Shimjith (srshim@barc.gov.in) is with Reactor Control System Design Section, Bhabha Atomic Research Centre, Mumbai, 400 085, India and Homi Bhabha National Institute, Mumbai, 400 094, India.

A. John Arul (arul@igcar.gov.in) is with Probabilistic Safety, Reactor Shielding and Nuclear Data Section, Indira Gandhi Centre for Atomic Research, Kalpakkam, 603 102, India.

Generally, a robust controller often has to spend high control energy to achieve satisfactory performance in an uncertain environment, which may sometimes lead to the saturation of actuators. Practically, a robust control strategy which spends less control energy is desired. This stimulus leads to the advancement of hybrid control strategies by integrating robust control with optimal control techniques [20]–[22], [28], [29]. SMC has been combined with optimal control to design core power control under the assumption that the complete state information is available for the control design [20], [22]. However, for instance, the concentration of delayed neutron precursors is not directly measurable in a reactor. Thus, a state estimator is required to estimate the unmeasurable states and to design the state feedback control strategy [17], [19].

In this paper, a new control strategy for a PWR-type NPP is proposed by combining the optimal LQG control and the robust ISM design approaches. The proposed LQG-ISM technique consists of the combined actions of a nominal controller and a discontinuous controller. The nominal controller uses the LQG approach, which involves a linear quadratic tracker (LQT) for state feedback control and a Kalman filter for states estimation. On the other hand, the discontinuous control employs the ISM approach, which allows the system motion to be invariant to disturbances throughout the entire system response. This paper further proposes a robust-optimal hybrid control strategy by integrating the LQG-ISM control with the LTR technique. The overall architecture thus offers enhanced robustness with improved system performance in the presence of parametric uncertainties and disturbances.

In NPP control design literature, the coupling effects among the reactor-core, steam generator, pressurizer, turbine-governor, and different piping and plenum are most often ignored while designing the individual controllers [1]–[26]. The dynamics of actuators and sensors are also frequently omitted. Pragmatically, it is meaningful to develop control methods for the whole NPP system. However, there are very few results for controlling an entire NPP [30], [31]. In this regard, the proposed work designs state feedback control techniques using estimated states for the integrated NPP model. Both proposed techniques are applied to different subsystems of a PWR-type NPP. In particular, the paper addresses the following problems: reactor power and temperature controls, steam generator pressure control, pressurizer pressure and level controls, and turbine speed control. The efficacy of the proposed work has been tested using simulations in the MATLAB/Simulink environment. The proposed techniques have been further compared with other classical techniques. The main contributions of the paper are listed below:

- Robust-optimal hybrid control techniques are proposed to improve system performance and robustness with minimum control efforts in the presence of parametric uncertainties and disturbances.
- Design, validation, and testing of the control technique is performed for various control loops of a PWR-type NPP.
- Reactor power control, temperature control, steam generator pressure control, pressurizer pressure and level controls, and turbine speed control problems are studied.

The remainder of the paper is organized as follows: Section II presents the dynamic non-linear model of PWR-type NPP. Section III formulates the control design problem. Section IV presents the proposed control scheme. Section V implements the proposed technique on the NPP and discusses its effectiveness through simulations. Conclusions are drawn in section VI indicating main contributions.

II. Dynamic Model of a PWR Nuclear Power Plant

The dynamic model of the PWR-type NPP is discussed in detail in [32].

A. Reactor Core Model

The core-neutronics model consisting of normalized power (P_n) and normalized precursor concentration of six groups of delayed neutrons (C_{in}) is given by,

$$\frac{dP_n}{dt} = \frac{\rho_t - \sum_{i=1}^{6} \beta_i}{\Lambda} P_n + \sum_{i=1}^{6} \frac{\beta_i}{\Lambda} C_{in}, \tag{1}$$

$$\frac{dC_{in}}{dt} = \lambda_i P_n - \lambda_i C_{in}, \qquad i = 1, 2, \ldots 6. \tag{2}$$

where λ_i and β_i are decay constant and fraction of delayed neutrons of i^{th} group, respectively. Λ is neutron generation time. The neutronic power in a reactor can be monitored using ex-core ion-chambers detectors, placed outside the core, and their associated amplifiers. The ex-core detector current (i_{lo}) is sensed using a logarithmic amplifier as [33]

$$\tau_1 \tau_2 \frac{d^2 i_{lo}}{dt^2} + (\tau_1 + \tau_2) \frac{di_{lo}}{dt} + i_{lo} = K_{lo} \log_{10} (\kappa_{lo} P_n). \tag{3}$$

where τ_1 and τ_2 are time constants of the logarithmic amplifier. K_{lo} is the gain of the logarithmic amplifier and κ_{lo} is a constant signifying the steady-state characteristics of the amplifier. The total reactivity (ρ_t) consists of reactivity due to rod movement (ρ_{rod}), and feedbacks due to variations in fuel temperature (T_f), coolant temperatures (T_{c1} and T_{c2}), and primary coolant pressure (p_p) as

$$\rho_t = \rho_{rod} + \alpha_f T_f + \alpha_c T_{c1} + \alpha_c T_{c2} + \alpha_p p_p, \tag{4}$$

$$\frac{d\rho_{rod}}{dt} = G v_{rod}, \tag{5}$$

where α_f, α_c, α_p are coefficient of reactivity due to feedbacks from fuel temperature, coolant temperature, and pressurizer pressure. G is reactivity worth of the regulating rod and v_{rod} is the rod movement speed.

B. Thermal-Hydraulics Model

The thermal-hydraulics model is governed by the Mann's model [34] which relates the core power to the temperature drop from fuel to coolant nodes,

$$\frac{dT_f}{dt} = H_f P_n - \frac{1}{\tau_f} (T_f - T_{c1}), \tag{6}$$

$$\frac{dT_{c1}}{dt} = H_c P_n + \frac{1}{\tau_c} (T_f - T_{c1}) - \frac{2}{\tau_r} (T_{c1} - T_{rxi}), \tag{7}$$

$$\frac{dT_{c2}}{dt} = H_c P_n + \frac{1}{\tau_c} (T_f - T_{c1}) - \frac{2}{\tau_r} (T_{c2} - T_{c1}), \tag{8}$$

where H_f and H_c denote the rate of rise of fuel and coolant temperature, respectively. τ_f, τ_c, and τ_r are time constants, which characterise the thermal lag in fuel, residence time in coolant, and in channel, respectively. The RTDs are used to sense the coolant temperature and its transmitter at the inlet (T_{rtd1}) and outlet (T_{rtd2}) as,

$$\frac{dT_{rtd1}}{dt} = \frac{1}{\tau_{rtd}}\left(-T_{rtd1} + 2T_{c1} - T_{rxi}\right), \tag{9}$$

$$\frac{dT_{rtd2}}{dt} = \frac{1}{\tau_{rtd}}\left(-T_{rtd2} + 2T_{c2} - T_{rxu}\right). \tag{10}$$

A current signal (i_{rtd}) can be obtained from the sensed RTD signals as

$$i_{rtd} = K_{rtd}\frac{(((T_{rtd1} + T_{rtd2})/2) - T_{rxi0})}{(T_{rxu0} - T_{rxi0})} + 4, \tag{11}$$

where K_{rtd} and τ_{rtd} are the gain and time constant of RTD, respectively.

C. Piping & Plenum Model

Hot-leg piping (T_{hot}), cold-leg piping (T_{cold}), reactor lower plenum (T_{rxi}), reactor upper plenum (T_{rxu}), steam generator inlet plenum (T_{sgi}), and steam generator outlet plenum (T_{sgu}) can be represented by first order ordinary differential equations as [34],

$$\frac{dT_{rxu}}{dt} = \frac{1}{\tau_{rxu}}\left(T_{c2} - T_{rxu}\right), \tag{12}$$

$$\frac{dT_{hot}}{dt} = \frac{1}{\tau_{hot}}\left(T_{rxu} - T_{hot}\right), \tag{13}$$

$$\frac{dT_{sgi}}{dt} = \frac{1}{\tau_{sgi}}\left(T_{hot} - T_{sgi}\right), \tag{14}$$

$$\frac{dT_{sgu}}{dt} = \frac{1}{\tau_{sgu}}\left(T_{p2} - T_{sgu}\right), \tag{15}$$

$$\frac{dT_{cold}}{dt} = \frac{1}{\tau_{cold}}\left(T_{sgu} - T_{cold}\right), \tag{16}$$

$$\frac{dT_{rxi}}{dt} = \frac{1}{\tau_{rxi}}\left(T_{cold} - T_{rxi}\right), \tag{17}$$

where τ_{rxu}, τ_{rxi}, τ_{hot}, τ_{cold}, τ_{sgu}, and τ_{sgi} denote time constants of reactor upper plenum, reactor lower plenum, hot-leg, cold-leg, steam generator outlet plenum, and steam generator inlet plenum, respectively.

D. Steam Generator Model

A five node configuration is used to represent the steam generator where the primary coolant lump (PCL) (T_{p1} and T_{p2}) and metal tube lump (MTL) (T_{m1} and T_{m2}) are represented by two nodes each [35],

$$\frac{dT_{p1}}{dt} = \frac{1}{\tau_{p1}}\left(T_{sgi} - T_{p1}\right) - \frac{1}{\tau_{pm1}}\left(T_{p1} - T_{m1}\right), \tag{18}$$

$$\frac{dT_{p2}}{dt} = \frac{1}{\tau_{p2}}\left(T_{p1} - T_{p2}\right) - \frac{1}{\tau_{pm2}}\left(T_{p2} - T_{m2}\right), \tag{19}$$

$$\frac{dT_{m1}}{dt} = \frac{1}{\tau_{mp1}}\left(T_{p1} - T_{m1}\right) - \frac{1}{\tau_{ms1}}\left(T_{m1} - T_{s}\right), \tag{20}$$

$$\frac{dT_{m2}}{dt} = \frac{1}{\tau_{mp2}}\left(T_{p2} - T_{m2}\right) - \frac{1}{\tau_{ms2}}\left(T_{m2} - T_{s}\right), \tag{21}$$

where τ_{p1} and τ_{p2} are time constants of PCL 1 and PCL 2, respectively. τ_{pm1} and τ_{pm2} denote the time constants to transfer coolant from PCL 1 to MTL 1 and PCL 2 to MTL 2, respectively. τ_{mp1} and τ_{mp2} denote the time constants to transfer coolant from MTL 1 to PCL 1 and MTL 2 to PCL 2, respectively. τ_{ms1} and τ_{ms2} denote the time constants to coolant transfer from MTL 1 to secondary coolant lump (SCL) and MTL 2 to SCL, respectively. The SCL represents steam pressure (p_s) by balancing mass, volume, and heat as,

$$\frac{dp_s}{dt} = \frac{1}{K_s}\left[U_{ms1}S_{ms1}\left(T_{m1} - T_s\right) + U_{ms2}S_{ms2}\left(T_{m2} - T_s\right) - \dot{m}_{so}\left(h_{ss} - c_{pfw}T_{fw}\right)\right], \tag{22}$$

where U_{ms1} and S_{ms1} denote the heat transfer coefficient and effective heat transfer area from MTL 1 to SCL. Similar definitions hold for U_{ms2} and S_{ms2}. c_{pfw} is specific heat of feedwater. T_{fw} is temperature of feedwater. The mass flow rate of steam ($\dot{m}_{so}$) is given by

$$\dot{m}_{so} = C_{tg}p_s \tag{23}$$

where C_{tg} is turbine-governor valve coefficient. K_s is a constant given by

$$K_s = m_{ws}\frac{\partial h_{ws}}{\partial p_s} + m_{ss}\frac{\partial h_{ss}}{\partial p_s} - m_{ws}\left(\frac{h_{ws} - h_{ss}}{\nu_{ws} - \nu_{ss}}\right)\frac{\partial \nu_{ss}}{\partial p_s} \tag{24}$$

where ν_{ws}, h_{ws}, and m_{ws} are specific volume, enthalpy, and mass of water in the secondary lump. Similarly, ν_{ss}, h_{ss}, and m_{ss} denote the parameters for steam in the secondary lump.

E. Pressurizer Model

The pressure (p_p) can be obtained by applying volume and energy balances of water and steam mixture with steam compressibility as [36],

$$\frac{dp_p}{dt} = \frac{\begin{array}{c} Q_{heat} + \dot{m}_{sur}\left(\frac{p_p\nu_s}{J_pC_{1p}} + \frac{h_{\bar{w}}}{C_{1p}}\right) + \\ \dot{m}_{spr}\left(h_{spr} - h_w + \frac{h_{\bar{w}}}{C_{1p}} + \frac{p_p\nu_w}{J_pC_{1p}}\right) \end{array}}{\begin{array}{c} m_w\left(K_{3p} + \frac{K_{4p}p_p}{J_p}\right) + \frac{m_sK_{4p}p_p}{J_p} - \\ \frac{V_w}{J_p} + \frac{C_{2p}}{C_{1p}}\left(h_{\bar{w}} + \frac{p_p\nu_s}{J_p}\right) \end{array}} \tag{25}$$

where Q_{heat} is rate of heat addition by heater, $\dot{m}_{spr}$ is mass spray flow rate, and $\dot{m}_{sur}$ is mass surge flow rate. The surge rate can be represented using coolant temperatures at different nodes as

$$\dot{m}_{sur} = \sum_{j=1}^{N} V_j\vartheta_j\frac{dT_j}{dt} \tag{26}$$

where V_j is volume and ϑ_j is slope of coolant density versus temperature curve for the j^{th} node.

The water level (l_w) in the pressurizer can be obtained by applying the mass balance equation on water and steam phase as,

$$\frac{dl_w}{dt} = \frac{1}{d_sA_p}\left(\left(A_p\left(l - l_w\right)K_{2p} - \frac{C_{2p}}{C_{1p}}\right)\frac{dp_p}{dt} + \frac{1}{C_{1p}^2}\left(C_{2p}\frac{dp_p}{dt} - \dot{m}_{sur} - \dot{m}_{spr}\right) + \frac{\dot{m}_{sur}}{C_{1p}}\right) \tag{27}$$

The intermediate variables are defined as

$$C_{1p} = \frac{d_w}{d_s} - 1; \tag{28}$$

$$C_{2p} = A_p\left(l - l_w\right)\frac{d_w}{d_s}K_{2p} + A_p l_w K_{1p}; \tag{29}$$

$$K_{1p} = \frac{\partial d_w}{\partial p_p}; K_{2p} = \frac{\partial d_s}{\partial p_p}; K_{3p} = \frac{\partial h_w}{\partial p_p}; K_{4p} = \frac{\partial \nu_s}{\partial p_p}. \tag{30}$$

where V_w is volume of water, J_p is conversion factor, A_p is cross-sectional area, l is length of pressurizer, h_{spr} is enthalpy of spray, and $h_{\bar{w}}$ is latent heat of vaporization. ν_w, h_w, d_w, and m_w denote the specific volume, enthalpy, density, and mass of water. Similarly, ν_s, d_w, and m_s denote the parameters for steam.

F. Turbine Model

The dynamical model of a turbine consisting of the high-pressure, intermediate-pressure, and low-pressure turbines is given by [37],

$$\begin{aligned}
&\frac{d^2P_{hp}}{dt} + \left(\frac{O_{rv}+\tau_{ip}}{\tau_{hp}\tau_{ip}}\right)\frac{dP_{hp}}{dt} + \left(\frac{O_{rv}}{\tau_{hp}\tau_{ip}}\right)P_{hp} = \left(\frac{O_{rv}F_{hp}}{\tau_{hp}\tau_{ip}}\right)\bar{\dot{m}}_{so} \\
&\qquad + \left(\frac{(1+\kappa_{hp})F_{hp}}{\tau_{hp}}\right)\frac{d\bar{\dot{m}}_{so}}{dt} \\
&\frac{d^2P_{ip}}{dt} + \left(\frac{O_{rv}\tau_{hp}+\tau_{ip}}{\tau_{hp}\tau_{ip}}\right)\frac{dP_{ip}}{dt} + \left(\frac{O_{rv}}{\tau_{hp}\tau_{ip}}\right)P_{ip} = \left(\frac{O_{rv}F_{ip}}{\tau_{hp}\tau_{ip}}\right)\bar{\dot{m}}_{so} \\
&\frac{d^3P_{lp}}{dt} + \left(\frac{O_{rv}\tau_{hp}+\tau_{ip}}{\tau_{hp}\tau_{ip}} + \frac{1}{\tau_{lp}}\right)\frac{d^2P_{lp}}{dt} + \left(\frac{O_{rv}(\tau_{lp}+\tau_{hp})+\tau_{ip}}{\tau_{hp}\tau_{ip}\tau_{lp}}\right) \\
&\qquad \frac{dP_{lp}}{dt} + \left(\frac{O_{rv}}{\tau_{hp}\tau_{ip}\tau_{lp}}\right)P_{lp} = O_{rv}F_{lp}\bar{\dot{m}}_{so}
\end{aligned} \tag{31}$$

where O_{rv} is valve opening degree. κ_{hp} is natural power overshooting coefficient of high-pressure turbine. P_{hp}, F_{hp}, and τ_{hp} denote the mechanical power output, fraction of steady-state power output, and volume time constant of high-pressure turbine, respectively. Similar definitions hold for P_{ip}, F_{ip}, and τ_{ip} of intermediate-pressure turbine and P_{lp}, F_{lp}, and τ_{lp} of low-pressure turbine.

The steam flow is $\bar{\dot{m}}_{so} = \dot{m}_{so}/\dot{m}_{sor}$, where $\dot{m}_{sor}$ is the rated steam mass flow rate. The steam flow rate can be modified using the turbine-governor valve coefficient as

$$\frac{d^2C_{tg}}{dt^2} + 2\zeta_{tg}\varpi_{tg}\frac{dC_{tg}}{dt} + \varpi_{tg}^2 C_{tg} = \varpi_{tg}^2 K_{tg}u_{tg} \tag{32}$$

where u_{tg} is the input signal to the valve, ζ_{tg} is damping ratio, ϖ_{tg} is natural frequency of oscillation, K_{tg} is gain of turbine governor valve. The total mechanical output of the turbine (P_{tur}) is computed as,

$$P_{tur} = P_{hp} + P_{ip} + P_{lp}. \tag{33}$$

The turbine-generator model also consists of a turbine speed system which produces the rate of change in turbine speed (ω_{tur}) in accordance with the difference in generator demand power (P_{dem}) and turbine output as

$$\frac{d\omega_{tur}}{dt} = \frac{P_{tur} - P_{dem}}{(2\pi)^2 J_{tur}\omega_{tur}I_{tg}}. \tag{34}$$

where J_{tur} is conversion factor and I_{tg} is moment of inertia.

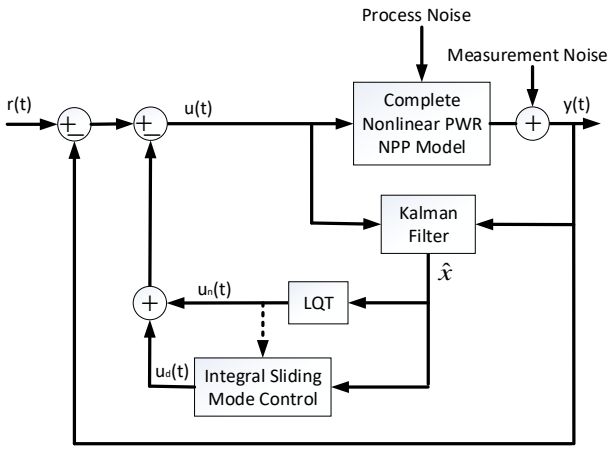

Fig. 1: Block diagram representation of the proposed hybrid control strategy.

III. Problem Formulation

Consider a linear time invariant system given by

$$\begin{aligned}
\dot{x}(t) &= Ax(t) + Bu(t) + B\xi(t) + \omega(t) \\
y(t) &= Cx(t) + \upsilon(t)
\end{aligned} \tag{35}$$

where $x(t) \in \mathbb{R}^n$, $u(t) \in \mathbb{R}^m$, $y(t) \in \mathbb{R}^l$, and $\xi(t) \in \mathbb{R}^m$ respectively represent state vector, control input, system output, and uncertainty. $\omega(t)$ and $\upsilon(t)$ are process noise and measurement noise with zero mean and covariance matrices $E\left(\omega(t)\omega(t)^\top\right) = \Xi$ and $E\left(\upsilon(t)\upsilon(t)^\top\right) = \Theta$, respectively. $A \in \mathbb{R}^{n\times n}$, $B \in \mathbb{R}^{n\times m}$, and $C \in \mathbb{R}^{l\times n}$ are system matrices. It is assumed that (A, B) is controllable and that the system uncertainties are unknown and bounded, so that

$$\|\xi(t)\| \leq \xi^*, \quad \xi^* > 0. \tag{36}$$

The control aim is to force the system output $y(t)$ to follow the desired reference $r(t)$ with minimal control effort in the presence of uncertainty $\xi(t)$. To achieve this objective the control scheme, depicted in Fig. 1, is proposed in this work, where the robust control reduces the effect of uncertainties and the optimal control guarantees minimum control effort. The control law $u(t)$ is formed of two parts, *i.e.*,

$$u(t) = u_n(t) + u_d(t) \tag{37}$$

where the nominal control ($u_n(t)$) is produced using LQG to obtain nominal system performance in an optimal way whereas the discontinuous control ($u_d(t)$) is generated by ISM to compensate for uncertainties. Thus, (35) can be written as

$$\begin{aligned}
\dot{x}(t) &= Ax(t) + B(u_n(t) + u_d(t) + \xi(t)) + \omega(t) \\
y(t) &= Cx(t) + \upsilon(t)
\end{aligned} \tag{38}$$

IV. Proposed Hybrid Control Design Scheme

A. Nominal Control Design

The nominal control uses the LQG approach, which involves two steps, state estimation using a Kalman filter and optimal state feedback control using the LQT.

1) Kalman Filter: The Kalman filter estimation problem is to find an optimal state estimate $\hat{x}(t)$ such that the following error covariance is minimized:

$$J_1 = \lim_{t\to\infty} E\left\{(x(t)-\hat{x}(t))\,(x(t)-\hat{x}(t))^\top\right\} \tag{39}$$

The Kalman filtering problem is estimated by computing the Kalman gain K_f given by

$$K_f = P_f C^\top \Theta^{-1} \tag{40}$$

where P_f is a symmetric positive semidefinite matrix and can be computed using a solution of following Algebraic Riccati Equation (ARE) as

$$AP_f + P_f A^\top + \Gamma\Xi\Gamma^\top - P_f C^\top \Theta^{-1} C P_f = 0 \tag{41}$$

where $\Gamma \in \mathbb{R}^{n\times m}$ is disturbance input matrix. Thus, the estimated states $\hat{x}(t)$ for the nominal system are given by,

$$\dot{\hat{x}}(t) = A\hat{x}(t) + Bu(t) + K_f(y(t) - C\hat{x}(t)). \tag{42}$$

2) Linear Quadratic Tracker: The classical linear quadratic regulator design is modified to track the reference signal. The LQT design computes an optimal control input by minimizing the cost function [38]:

$$J_2 = \int_0^\infty \left((C\hat{x}(t)-r(t))^\top Q\,(C\hat{x}(t)-r(t)) + u_n(t)^\top R u_n(t)\right) d\tau \tag{43}$$

where Q and R are positive semidefinite and positive definite weighing matrices, respectively. Thus, the state feedback control law is given by,

$$u_n(t) = -K_c\hat{x}(t) + K_v s(t) \tag{44}$$

where the optimal feedback gain K_c is computed by finding a solution of the following ARE

$$A^\top P_c + P_c A + C^\top Q C - P_c B R^{-1} B^\top P_c = 0 \tag{45}$$

It is given by

$$K_c = R^{-1}B^\top P_c \tag{46}$$

where P_c is a symmetric positive semidefinite matrix. The feed-forward gain K_v is computed as

$$K_v = R^{-1}B^\top \tag{47}$$

and $s(t)$ is given by the solution of

$$-\dot{s}(t) = (A - BK_c)^\top s(t) + C^\top Q r\,(t)\,, s\,(\infty) = 0 \tag{48}$$

Thus, the optimal state feedback nominal control law is then implemented using the estimated states as

$$u_n(t) = -R^{-1}B^\top P_c\hat{x}(t) + R^{-1}B^\top s(t) \tag{49}$$

B. Loop Transfer Recovery

Due to the incorporation of a Kalman filter for state estimation, the robustness and stability margin of the nominal control is weakened [39]. To resolve this, either the gain of the Kalman filter or the gain of the tracker can be modified using the LTR approach. The gains are shaped so that the resultant filter transfer function has guaranteed stability margins. The open-loop system with the LQG return ratio at the input is given by

$$G(s) = K_c\,(sI - A + BK_c + K_f C)^{-1}\,K_f C(sI-A)^{-1}B \tag{50}$$

The LTR at the input can be designed as follows: First, the LQT is designed by suitably selecting Q and R. Then, $\Gamma = B$, $\Xi = q\Xi$ and $\Theta = I$ are selected. The idea of LTR design is to use a fictitious gain coefficient q and then gradually increase $q\to\infty$, such that the final loop-transfer function approximates to the state-feedback loop transfer function designed by the LQT as

$$\lim_{q\to\infty} G(s) = K_c\,(sI-A)^{-1}\,B \tag{51}$$

The proposed LQG/LTR-ISM scheme first designs the nominal control using LQG and enhances the stability using the LTR technique and then combines with the ISM approach. Thus, the hybrid approach possesses strong robustness capability with enhanced performance.

C. Discontinuous Control Design

The ISM works by designing first an integral sliding surface followed by the design of a discontinuous control law. An integral sliding surface $\phi(t) \in \mathbb{R}^m = \begin{bmatrix}\phi_1(t)\ \phi_2(t)\ \cdots\ \phi_m(t)\end{bmatrix}^\top$ can be designed as [27],

$$\phi(t) = G\left[\hat{x}(t) - \hat{x}(0) - \int_0^\top \dot{\hat{x}}_n(\tau)\ d\tau\right] \tag{52}$$

where $G \in \mathbb{R}^{m\times n}$ is the design freedom. For simplicity, it is selected as left-pseudo inverse of input distribution matrix B given as

$$G = (B^\top B)^{-1}B^\top \tag{53}$$

The term $-\hat{x}(0)$ assures that the system starts from the sliding surface by eliminating the reaching phase and enforcing $\phi(0) = 0$. Thus, the closed-loop system turns out to be robust towards matched uncertainties from the initial time instant. Here, the discontinuous control $u_d(t)$ is formulated based on the reachability condition as [40]

$$u_d(t) = -\mu\ \mathrm{sign}(\phi(t)) \tag{54}$$

where μ is an appropriately designed positive constant and $\mathrm{sign}(.)$ is the standard signum function.

D. Stability Analysis

A Lyapunov function $V(t)$ is selected as [41]

$$V(t) = \frac{1}{2}\phi^\top(t)\phi(t) \tag{55}$$

Differentiating $V(t)$ with respect to time gives

$$\dot{V}(t) = \phi^\top(t)\dot{\phi}(t) = \phi^\top(t)G\left(\dot{\hat{x}}(t) - \dot{\hat{x}}_n(t)\right) \tag{56}$$

TABLE I: Tuning parameters for different control approaches

Configuration			LQG				LTR	ISM
Case	Input	Output	Q	R	Ξ	Θ	q	μ
A.1	v_{rod}	i_{lo}	1×10^{-3}	1×10^{5}	$5\times10^{-3}I_n$	1	1×10^{6}	10^{-1}
A.2	v_{rod}	i_{lo}	1×10^{-3}	1×10^{5}	$5\times10^{-3}I_n$	1	1×10^{6}	10^{-1}
B	v_{rod}	i_{rtd}	1×10^{-3}	1×10^{5}	$5\times10^{-4}I_n$	1	1×10^{9}	10^{-1}
C	u_{tg}	p_s	1×10^{-3}	1×10^{0}	$5\times10^{-3}I_n$	1	1×10^{6}	10^{-1}
D.1	Q_{heat}	p_p	1×10^{-2}	1×10^{-7}	$5\times10^{-5}I_n$	1	1×10^{18}	10^{0}
D.2	$\dot{m}_{spr}$	p_p	1×10^{-2}	1×10^{-5}	$5\times10^{-5}I_n$	1	1×10^{15}	10^{0}
D.3	$\dot{m}_{sur}$	l_w	1×10^{-2}	1×10^{-6}	$5\times10^{-3}I_n$	1	1×10^{12}	10^{0}
E	u_{tg}	ω_{tur}	1×10^{2}	1×10^{-2}	$5\times10^{-3}I_n$	1	1×10^{4}	10^{-1}

During sliding mode, the system trajectories follow the nominal system trajectories *i.e.*, $\hat{x}(t)=\hat{x}_n(t)$. Thus, (56) becomes

$$\begin{aligned}\dot{V}(t) &= \phi^\top(t)\left(u_d(t)+\xi(t)\right) = \phi^\top(t)\left(-\mu\ \mathrm{sign}(\phi(t))+\xi(t)\right)\\ &= -\mu\phi^\top(t)\mathrm{sign}(\phi(t))+\phi^\top(t)\xi(t)\\ &\le -\mu\|\phi\left(t\right)\|+\|\phi\left(t\right)\|\|\xi\left(t\right)\|\\ &\le \|\phi\left(t\right)\|\big(-\mu+\xi^*\big)\end{aligned} \tag{57}$$

Thus, for any choice of $\mu\ge\xi^*+\delta$, (57) becomes

$$\dot{V}(t)=\phi^\top(t)\dot{\phi}(t)\le-\delta\|\phi\left(t\right)\| \tag{58}$$

where δ is a small positive constant.

It is apparent from (58) that the trajectories of the uncertain system will be maintained on the sliding surface $\phi(t)=0$ and drives towards the specified equilibrium point despite the uncertainties in finite time. The boundary layer approach can be used to restrain the effect of chattering due to the presence of the signum function [41]. The signum function can be approximated as,

$$\mathrm{sign}\left(\phi_i\left(t\right)\right)=\frac{\phi_i\left(t\right)}{\left|\phi_i\left(t\right)\right|+\varepsilon}\qquad i=1,2,\cdots m \tag{59}$$

where ε is a small positive constant. The boundary layer technique may results in loss of invariance property and steady state error proportional to boundary layer thickness. Thus, for good performance the value of ϵ should be selected as small as possible [40]. A more prominent approach to reduce the effect of chattering is higher order sliding mode control.

V. Result and Discussion

The simulation results show the performance tests of the designed controllers under various conditions. The controllers are designed after linearizing the nonlinear system operating at 100% full power (FP). The steady-state values of different variables at the operating point are given in Table A.1. The controllers are then tested on the nonlinear PWR-type NPP model under external disturbances and parametric uncertainties [20]–[22]. Here, a sum of sinusoids is considered as external disturbance ($\xi(t)$) and a linear chirp signal is considered as parametric uncertainty ($\sigma(t)$). These are given by

$$\begin{aligned}\xi(t)=\xi_0\big(&5\sin(10^{-4}t)+3\sin(10^{-3}t)+2\sin(10^{-2}t)\\&+\sin(10^{-1}t)\big)\end{aligned} \tag{60}$$

$$\sigma(t)=\sigma_0\sin\left(2\pi\times10^{-4}t+4.95\pi\times10^{-6}t^2\right) \tag{61}$$

The following key control loops are considered: reactor core power loop, temperature loop, steam generator loop, pressurizer pressure and level loop, and turbine speed loop. In each case, the results of the proposed control schemes are compared with other classical state feedback techniques such as LQG and LQG/LTR schemes. The controller tuning parameters and the definition of input and output vectors for every single-input single-output control loop are given in Table I.

The tracking performance is numerically compared using the percentage root mean squared error (PRMSE), which is calculated based on tracking error. The control performance is compared by computing the total variation of input (TVI) which is a measure of smoothness of the signal and the $\mathcal{L}_2$-norm of input ($\mathcal{L}_2$NI) which is a measure of spent control energy. These are given by

$$PRMSE=\sqrt{\frac{1}{N}\sum_{i=1}^{N}\left(y_i-r_i\right)^2}\times100\%, \tag{62}$$

$$TVI=\sum_{i=1}^{N}|u_{i+1}-u_i|, \tag{63}$$

$$\mathcal{L}_2NI=\sqrt{\sum_{i=1}^{N}\left(u_i\right)^2} \tag{64}$$

where N denotes the total number of samples, which is equal to simulation time divided by sampling interval.

A. Reactor Power Loop

The performance of the designed controllers is tested for typical load-following transients of a PWR-type NPP in the presence of disturbances and parametric uncertainties. The disturbance, $\xi(t)$, is in the rod speed with magnitude $\xi_0=10^{-4}$ and the parametric uncertainty, ($\sigma(t)$), is in total reactivity with magnitude $\sigma_0=10^{-4}$.

1) Case I: Initially, the NPP is assumed to be operating at 100% FP. A load-following transient is considered to study typical power variations in which the reference power is varied

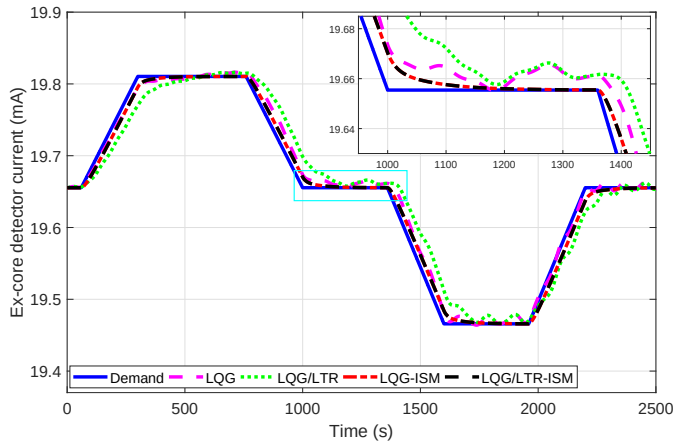

(a) Ex-core detector current.

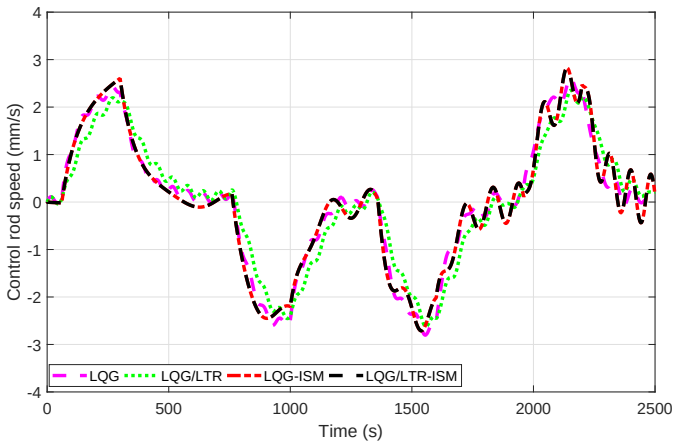

(b) Control rod speed movement.

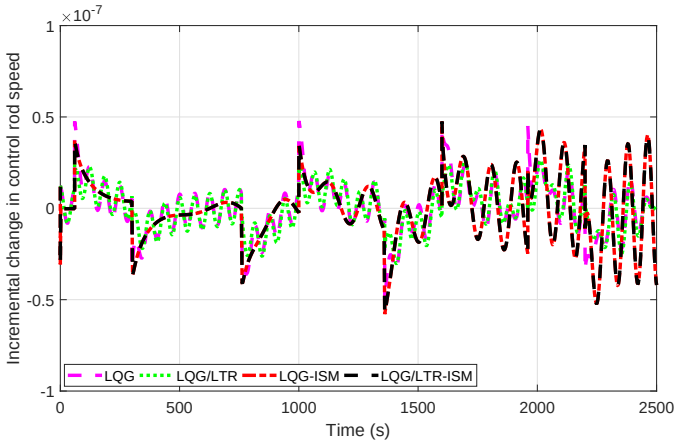

(c) Incremental change in control rod speed.

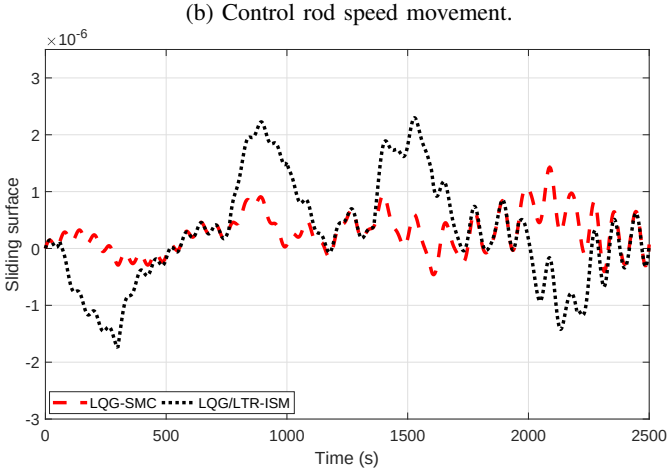

(d) Sliding surface.

Fig. 2: Variation of reactor power signals during the load-following mode of operation.

at 5%/min. It is given as follows:

$$P_n^{ref} = \begin{cases} 1, & 0 \le t \le 60 \\ 0.05(t-60)/60 + 1, & 60 < t \le 300 \\ 1.2, & 300 < t \le 760 \\ -0.05(t-760)/60 + 1.2, & 760 < t \le 1000 \\ 1, & 1000 < t \le 1360 \\ -0.05(t-1360)/60 + 1, & 1360 < t \le 1600 \\ 0.8, & 1600 < t \le 1960 \\ 0.05(t-1960)/60 + 0.8, & 1960 < t \le 2200 \\ 1, & 2200 < t \le 2500 \end{cases} \quad (65)$$

The performance of the controllers in terms of measured log-amplified ex-core detector current corresponding to output power is shown in Fig. 2a. The variations of control signal and the incremental change in control signal are shown in Figs. 2b and 2c, respectively. Variation of sliding surfaces using LQG-ISM and LQG/LTR-ISM is shown in Fig. 2d. It can be noted that LQG and LQG/LTR controllers are unable to reject the disturbances whereas, LQG-ISM and LQG/LTR-ISM controllers can track the set-point variations smoothly as envisaged. The disturbances are present in the control inputs of LQG and LQG/LTR controllers which may lead to wear, tear, and saturation of the actuators. The performance of LQG/LTR is slightly better than the LQG however, both techniques are unable to provide the desired response in the presence of disturbances and parametric uncertainties. The response of the proposed controllers is much-improved and free from disturbances. Table II compares the control performances of different schemes. The value of PRMSE for the LQG/LTR-ISM approach is lower than those of the other approaches. The LQG-ISM and LQG/LTR-ISM schemes take similar control efforts in terms of TVI and the $\mathcal{L}_2$NI and which are lower than that taken by the LQG and LQG/LTR techniques.

2) Case II: Another load-following transient is considered to validate the performance during a sudden load-decrement. The reference power value is brought down from 100% to 50% FP in a step manner and then it is slowly brought back to its initial steady-state value power at 5%/min. The transient is given as follows:

$$P_n^{ref} = \begin{cases} 1.0, & 0 \le t \le 200 \\ 0.5, & 200 < t \le 900 \\ 0.05(t-900)/60 + 0.5, & 900 < t \le 1200 \\ 0.75, & 1200 < t \le 1700 \\ 0.05(t-1700)/60 + 0.75, & 1700 < t \le 2000 \\ 1.0, & 2000 < t \le 2500 \end{cases} \quad (66)$$

The performance of the controllers in terms of measured log-amplified ex-core detector current is shown in Fig. 3a. The

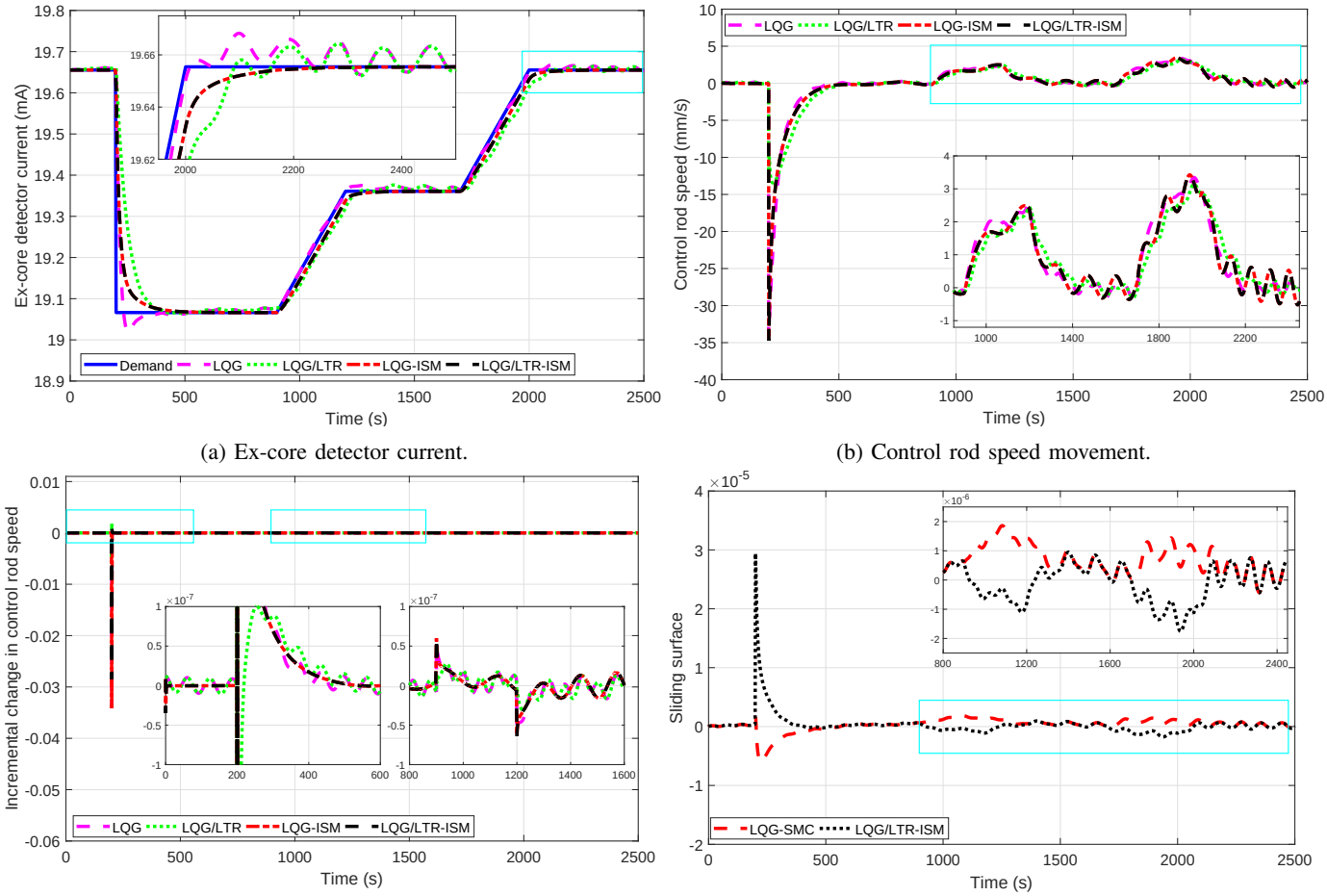

(a) Ex-core detector current.

(b) Control rod speed movement.

(c) Incremental change in control rod speed.

(d) Sliding surface.

Fig. 3: Variation of reactor power signals during the load-following mode of operation.

variations of control signal and the incremental change in control signal are shown in Figs. 3b and 3c, respectively. Variation of sliding surfaces using LQG-ISM and LQG/LTR-ISM is shown in Fig. 3d. The LQG/LTR controller gives better performance than the LQG controller where the latter gives large overshoot, however, both are unable to handle parametric uncertainties and disturbances which are found to present in the control inputs. The LQG-ISM and LQG/LTR-ISM can track the sudden load rejection transient without any overshoot and can reject the disturbances present in the system. The LQG-ISM and LQG/LTR-ISM are found to give better control performance over the LQG and LQG/LTR approaches. From Table II, it can be seen that the LQG/LTR-ISM approach tracks the demand set-point with minimum PRMSE. The LQG-ISM and LQG/LTR-ISM schemes take similar control efforts in terms of TVI and the $\mathcal{L}_2$NI and which are lower than that taken by the LQG and LQG/LTR techniques.

B. Temperature Control Loop

The NPP power can also be controlled using the coolant temperature. To analyse the performance of temperature control, in the presence of disturbances and parametric uncertainties similar to V-A, a load-following transient is considered as follows:

$$P_n^{ref} = \begin{cases} 1, & 0 \le t \le 60 \\ -0.05(t-60)/60 + 1, & 60 < t \le 300 \\ 0.8, & 300 < t \le 760 \\ 0.05(t-760)/60 + 0.8, & 760 < t \le 1000 \\ 1, & 1000 < t \le 1360 \\ 0.05(t-1360)/60 + 1, & 1360 < t \le 1600 \\ 1.2, & 1600 < t \le 1960 \\ -0.05(t-1960)/60 + 1.2, & 1960 < t \le 2200 \\ 1, & 2200 < t \le 2500 \end{cases} \quad (67)$$

The performance of the controllers, in terms of measured RTD current corresponding to the output power, is shown in Fig. 4a. Variation of the control signal and the incremental change in the control signal are shown in Figs. 4b and 4c, respectively. Variation of sliding surfaces using the LQG-ISM and LQG/LTR-ISM is shown in Fig. 4d. The LQG-ISM and LQG/LTR-ISM controllers can track the variation smoothly in the presence of disturbances and uncertainties, however, the LQG and LQG/LTR controllers are unable to do so and disturbances are found to be present in their control inputs. Table II shows that the LQG-ISM and LQG/LTR-ISM schemes spent lower control efforts in terms of $\mathcal{L}_2$NI and gave smoother signals in terms of TVI over other schemes. The PRMSE for

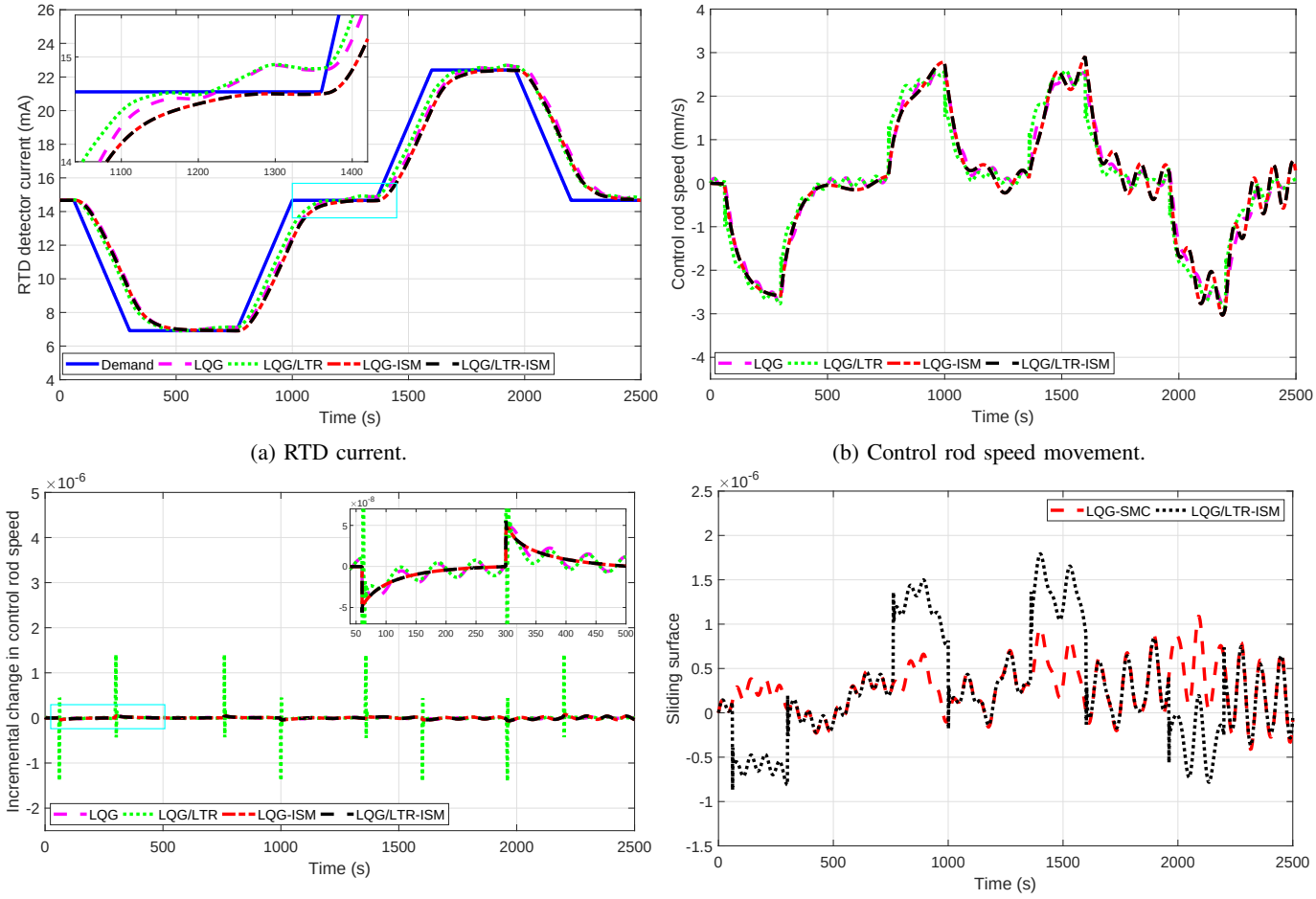

(a) RTD current.

(b) Control rod speed movement.

(c) Incremental change in control rod speed.

(d) Sliding surface.

Fig. 4: Variation of reactor temperature signals during the load-following mode of operation.

the LQG/LTR-ISM approach is found to be lower than those of the other approaches.

C. Steam Generator Loop

The performance of the designed controllers is tested for a set-point change in steam generator pressure in the presence of disturbances and parametric uncertainties. The disturbance, $\xi(t)$, is in the input signal to the turbine-governor valve with magnitude $\xi_0 = 10^{-3}$ and the parametric uncertainty, $(\sigma(t))$, is in turbine-governor valve coefficient with magnitude $\sigma_0 = 10^{-4}$. A set-point change in secondary pressure is applied as follows:

$$p_s^{ref} = \begin{cases} 7.285, & 0 \leq t \leq 200 \\ 0.01(t-200)/60 + 7.285, & 200 < t \leq 500 \\ 7.335, & 500 < t \leq 1200 \\ -0.01(t-1200)/60 + 7.335, & 1200 < t \leq 1500 \\ 7.285, & 1500 < t \leq 2000 \end{cases} \quad (68)$$

The performance of the controllers is shown in Fig. 5a. The variations of control signal and the incremental change in control signal are shown in Figs. 5b and 5c, respectively. Variation of sliding surfaces for LQG-ISM and LQG/LTR-ISM is shown in Fig. 5d. It can be observed that the LQG-ISM and LQG/LTR-ISM can track the variations smoothly in the presence of disturbances and parametric uncertainties. On the contrary, the LQG and LQG/LTR controllers are unable to reject the disturbances. From Table II, it can be seen that the PRMSE for the LQG/LTR-ISM approach is lower than those of the other approaches. The LQG-ISM and LQG/LTR-ISM schemes take similar control efforts in terms of $\mathcal{L}_2$NI which are significantly lower than those of the other approaches. Besides, the proposed control techniques produce smooth control signal in terms of TVI.

D. Pressurizer Loop

The pressurizer pressure control is usually achieved by actuating a bank of heaters and by adjusting the spray flow rate. The performance of the designed controllers is tested for a set-point change in pressurizer pressure in the presence of disturbances and parametric uncertainties. The disturbance, $\xi(t)$, is in the input signal to the actuator with magnitude $\xi_0 = 10^{-1}$ and the parametric uncertainty, $(\sigma(t))$, is in surge flow rate with magnitude $\sigma_0 = 10^{-4}$.

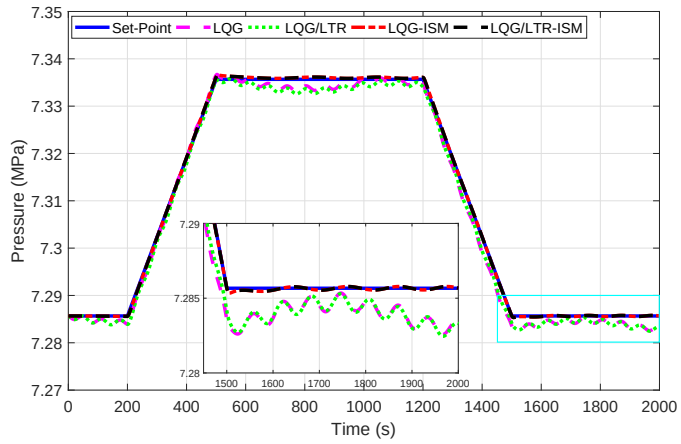

(a) Steam generator secondary pressure.

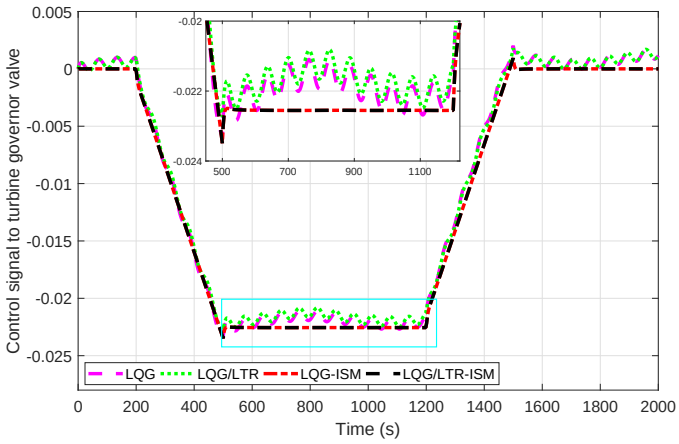

(b) Control signal to turbine governor valve.

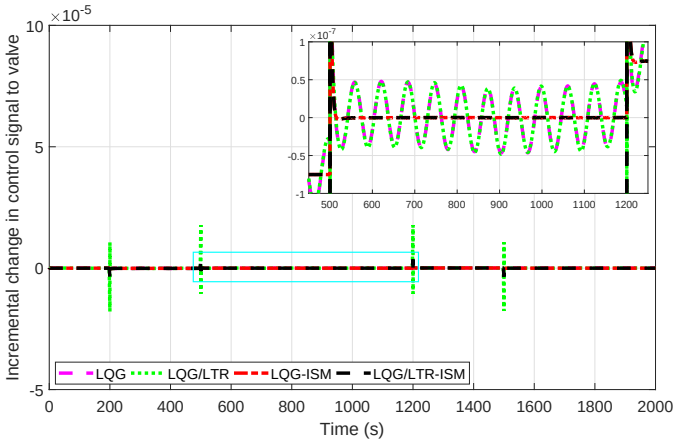

(c) Incremental change in control signal to valve.

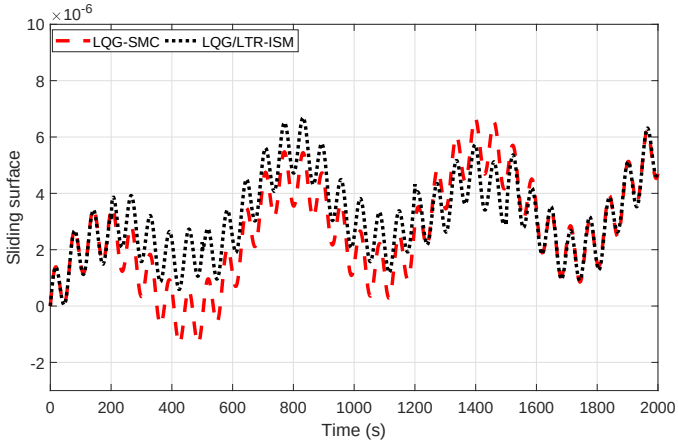

(d) Sliding surface.

Fig. 5: Variation of steam generator signals during a set-point change in secondary pressure.

1) Pressure Control by Heater: A set-point change in the pressurizer pressure is applied as follows:

$$p_p^{ref} = \begin{cases} 15.41, & 0 \leq t \leq 400 \\ 10^{-4}(t-400) + 15.41, & 400 < t \leq 500 \\ 15.42, & 500 < t \leq 2000 \end{cases} \quad (69)$$

The performance of the controllers is shown in Fig. 6a. It can be observed that all the controllers can track the set-point variations however, the LQG and LQG/LTR controllers are unable to reject the disturbances whereas, the LQG-ISM and LQG/LTR-ISM are able to effectively handle the disturbances and parametric uncertainties. The disturbances are found to be present in the control input and output of the LQG and LQG/LTR controllers. Variation of the control signal and the incremental change in the control signal are shown in Figs. 6b and 6c, respectively. Variation of sliding surfaces using LQG-ISM and LQG/LTR-ISM is shown in Fig. 6d. Table II shows that all the control schemes are found to take similar control energy in terms of $\mathcal{L}_2$NI. The LQG-ISM and LQG/LTR-ISM take minimum control variations in terms of TVI. The PRMSE for the LQG/LTR-ISM approach is found to be lower than those of the other approaches.

2) Pressure Control by Spray: A set-point change in the pressurizer pressure is applied as follows:

$$p_p^{ref} = \begin{cases} 15.41, & 0 \leq t \leq 400 \\ -10^{-4}(t-400) + 15.41, & 400 < t \leq 500 \\ 15.40, & 500 < t \leq 2000 \end{cases} \quad (70)$$

The performance of the proposed controller is shown in Fig. 7a. It can be observed that LQG and LQG/LTR controllers are able to track the set-point with superimposed disturbances. The LQG-ISM and LQG/LTR-ISM can reject the disturbances and parametric uncertainties and are able to smoothly track the set-point variation. The variations of control signal and the incremental change in control signal are shown in Figs. 7b and 7c, respectively. Variation of sliding surfaces using LQG-ISM and LQG/LTR-ISM is shown in Fig. 7d. The control efforts taken by LQG-ISM and LQG/LTR-ISM are found to be lower than that of the other approaches. From Table II, it is clear that the LQG-ISM and LQG/LTR-ISM scheme spent lower control energies in terms of $\mathcal{L}_2$NI and give smoother variation in terms of TVI. The PRMSE for the LQG/LTR-ISM approach is found to be lower than those of the other approaches.

3) Level Control: The pressurizer level control system maintains the water level for the reactor core coolant system. A

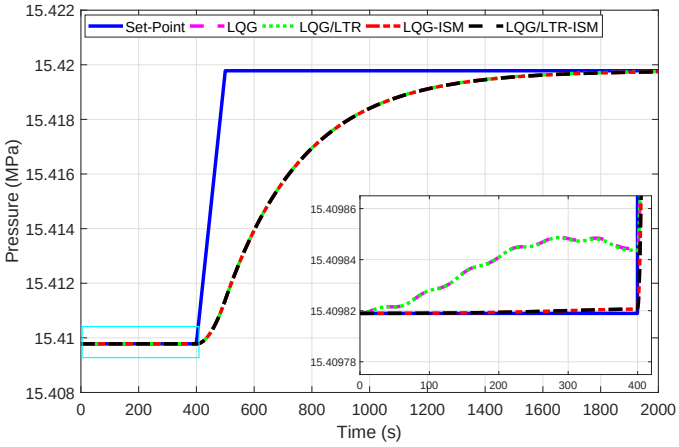

(a) Pressurizer pressure.

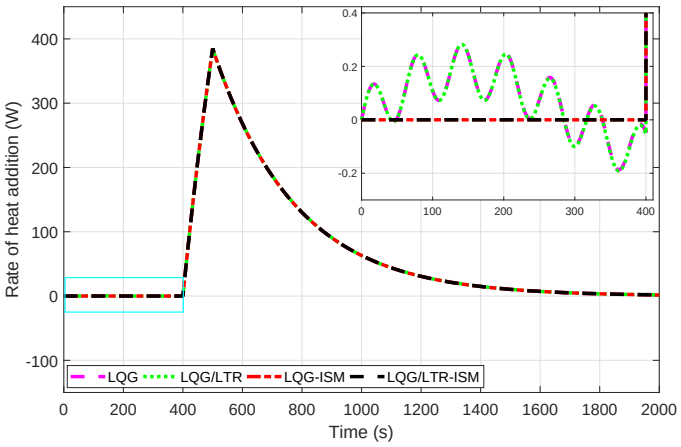

(b) Rate of heat addition.

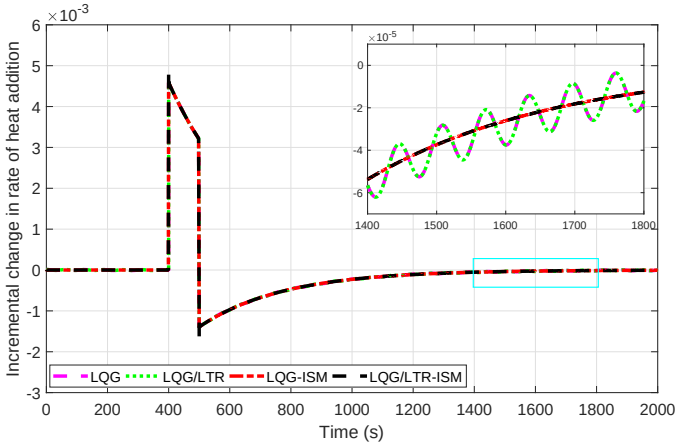

(c) Incremental change in rate of heat addition.

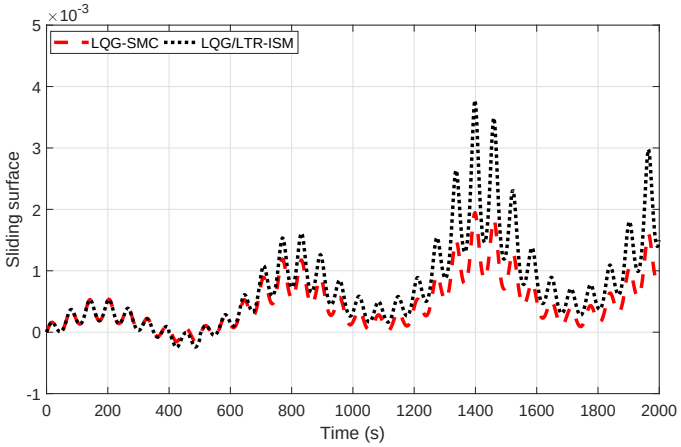

(d) Sliding surface.

Fig. 6: Variation of pressurizer heater signals during a set-point change in pressure.

set-point change in the pressurizer level is applied as follows:

$$l_w^{ref} = \begin{cases} 28.06, & 0 \leq t \leq 250 \\ -0.001(t-250)+28.06, & 250 < t \leq 500 \\ 27.81, & 500 < t \leq 1000 \\ 0.001(t-1000)+27.81, & 1000 < t \leq 1250 \\ 28.06, & 1250 < t \leq 2000 \end{cases} \quad (71)$$

The performance of the controllers is shown in Fig. 8a. The LQG-ISM and LQG/LTR-ISM can track the set-point variation smoothly in the presence of disturbances and uncertainties whereas the LQG and LQG/LTR controllers are unable to reject the disturbances. The variation of control signal and the incremental change in control signal are shown in Figs. 8b and 8c, respectively. Variation of sliding surfaces using LQG-ISM and LQG/LTR-ISM is shown in Fig. 8d. Table II shows that the LQG-ISM and LQG/LTR-ISM spent lower control energies than that of the other approaches. The value of PRMSE and $\mathcal{L}_2$NI are found to be at their minimum for the LQG/LTR-ISM technique whereas the LQG-ISM approach takes minimum TVI.

E. Turbine Speed Loop

The turbine speed control system regulates the shaft speed by controlling the steam flow to the turbine through the turbine governor valve. The performance of the proposed technique is tested by regulating the demand power using turbine speed in the presence of disturbances and parametric uncertainties similar to V-C. The demand power from the generator is varied at 10%/min. It is given as follows:

$$P_{dem}^{ref} = \begin{cases} 1, & 0 \leq t \leq 80 \\ -0.1(t-80)/60+1, & 80 < t \leq 200 \\ 0.8, & 200 < t \leq 1180 \\ 0.1(t-1180)/60+0.8, & 1180 < t \leq 1300 \\ 1, & 1300 < t \leq 2500 \end{cases} \quad (72)$$

The performance of the proposed controllers for tracking the set-point change in demand power is shown in Fig. 9a. The LQG and LQG/LTR controllers track the variation with disturbances superimposed on the control input and output. The LQG-ISM and LQG/LTR-ISM can track the set-point variation smoothly in the presence of disturbances and parametric uncertainties. The variation in turbine speed is shown in Fig. 9b. The variation of control signal and the incremental change in control signal are shown in Figs. 9c and 9d, respectively. From Table II, it can be noticed that the LQG/LTR approach tracks the demand set-point with minimum PRMSE however, it is not able to reject the disturbances. The LQG-ISM and LQG/LTR-ISM schemes take similar control efforts in terms of $\mathcal{L}_2$NI

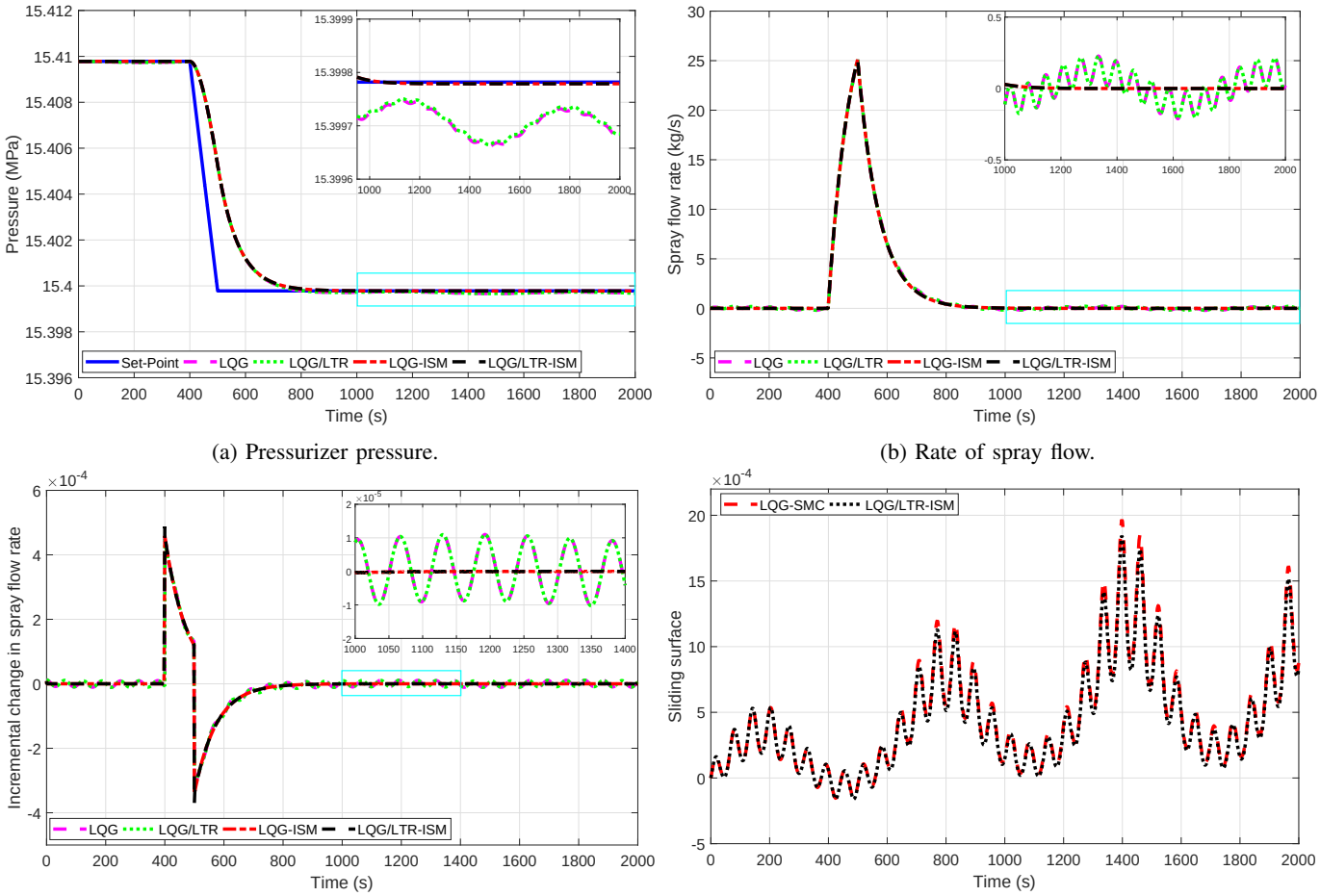

(a) Pressurizer pressure.

(b) Rate of spray flow.

(c) Incremental change in rate of spray flow.

(d) Sliding surface.

Fig. 7: Variation of pressurizer spray flow signals during a set-point change in pressure.

which are lower than those taken by the LQG and LQG/LTR techniques. Proposed techniques give smooth control signal variation in terms of TVI.

F. Discussion

Pressurized water-type nuclear power plants are complex nonlinear systems that exhibit significant uncertainties in their dynamic behaviour. Uncertainties that enter the system through its input channels fall under the category of matched uncertainties. Examples of matched uncertainties include actuator faults or degradation, sudden variation in rod position or speed, and changes in valve coefficients. Unmatched uncertainties, on the other hand, are those uncertainties that do not affect the system through its input channels. In the case of a nuclear reactor, both matched and unmatched uncertainties are always present in addition to parametric uncertainties in the system. Thus, for their safe, stable, and efficient operation, it is relevant to develop robust control techniques for nuclear power plants. The proposed technique makes the closed-loop system robust by automatically overcoming matched uncertainties. It can further compensate for parametric uncertainties. The proposed control scheme exhibits robustness from the very beginning of the system response following a matched disturbance and rejects such disturbances with less control effort as compared to conventional controllers like PID [33], SMC [41], LQG [38], and LQG/LTR [2]. Although the proposed control strategy is not suitable to compensate for unmatched uncertainties, it can be combined with other techniques, such as a disturbance observer, to reduce the impact of unmatched disturbances. Due to its simple structure, the proposed control scheme can be combined with existing state-feedback controllers as an additional control routine running on a digital control system, and thus it is likely to be well suited for practical implementation once the required certifications and verifications are passed.

From the simulation results, it has been observed that the LQG/LTR-ISM approach gives the least tracking error and takes the least control energy in tracking the set-point whereas the LQG-ISM approach gives the smallest variation in the control input. In the case of LQG, the Q and R matrices regulate the penalties on the states variables and control input, respectively, and determine the location of poles of the closed-loop system. Thus, they are selected such that the set-point can be tracked quickly without any overshoot. In the case of LTR, the recovery gain q is selected based on the frequency response of the target feedback loop. The value of q is selected such that the loop transfer function approaches the ideal return ratio given by the target feedback loop. The tuning parameter of ISM is selected to ensure that the discontinuous control

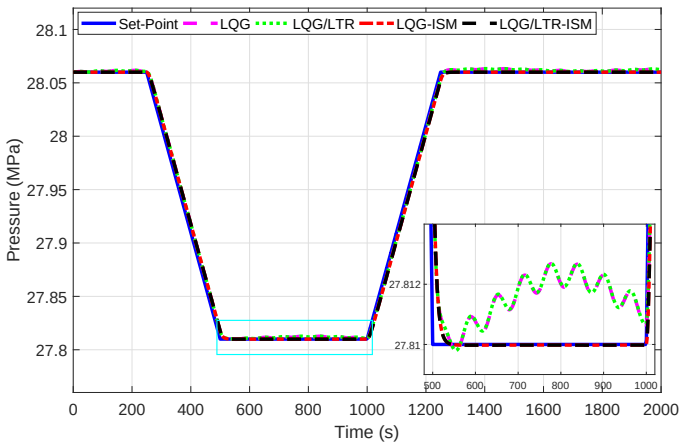

(a) Pressurizer level.

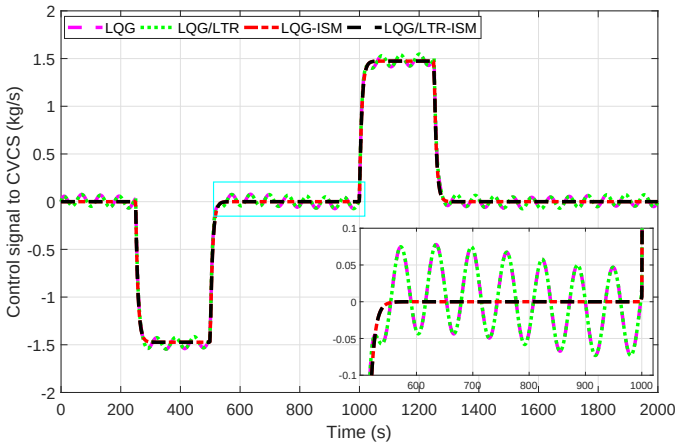

(b) Control signal to CVCS system.

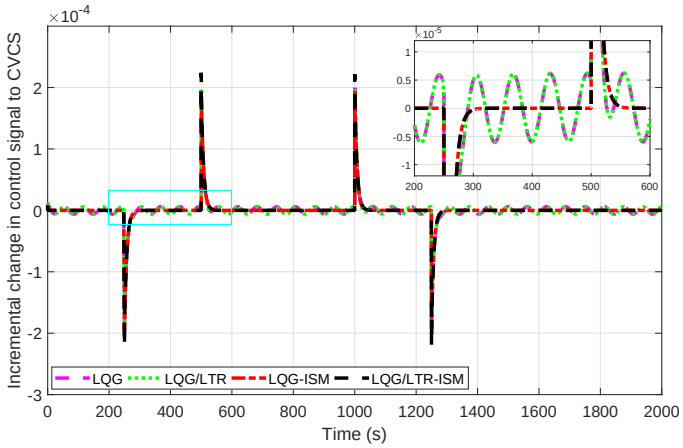

(c) Incremental change in control signal to CVCS.

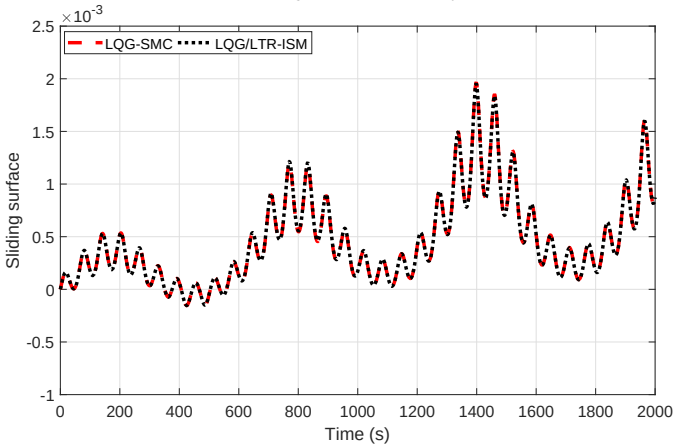

(d) Sliding surface.

Fig. 8: Variation of pressurizer level signals during a set-point change in level.

signal does not contain high-frequency noise. Based on these criteria, different controllers have been tuned for the different cases under consideration, as reflected in Table I.

VI. Conclusions

This work proposes state feedback-based hybrid control design techniques by integrating robust-optimal approaches for the control of a pressurized water-type nuclear power plant. The linear quadratic Gaussian (LQG) control is combined with the integral sliding mode (ISM) technique. A robust-optimal hybrid control technique further combines the LQG-ISM approach with the loop transfer recovery technique. The control architecture thus offers enhanced robustness with improved performance and tracks the reference set-point smoothly in the presence of disturbances and parametric uncertainties. The effectiveness of the techniques has been validated using simulations on different subsystems of the PWR-type NPP. The control performances of the proposed approaches have been quantitatively compared with LQG and LQG/LTR control approaches using different numerical measures for the reactor power control, temperature control, steam generator pressure control, pressurizer pressure and level controls, and turbine speed control. The proposed controllers can handle disturbances and parametric uncertainties in the system and they have been found to give a better performance over other controllers.

VII. Acknowledgement

The work presented in this paper has been financially supported under grants EP/R021961/1 and EP/R022062/1 from the Engineering and Physical Sciences Research Council.

Appendix

The parameters listed in the Table A.1 [32] correspond to a typical Westinghouse-type PWR. The parameters have been collected from the available literature on PWR-type plants [34]–[37], Westinghouse documentation [42], and steam tables [43].

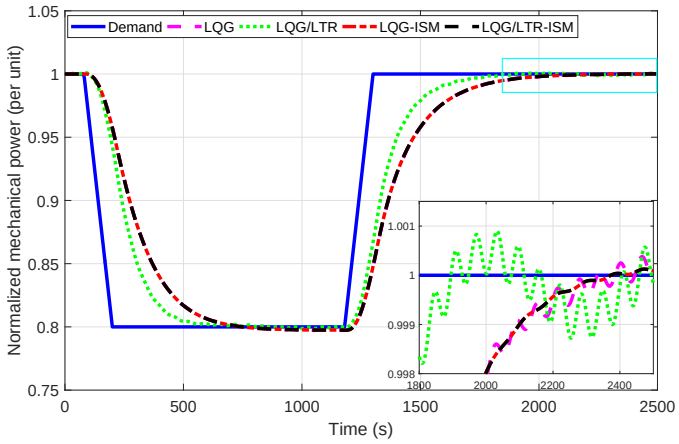

(a) Normalized mechanical power.

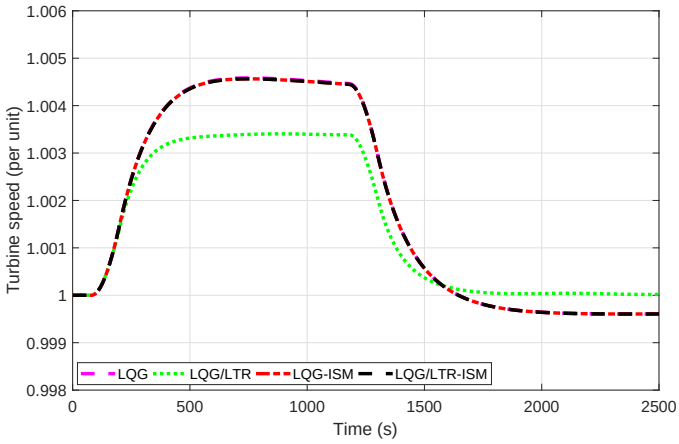

(b) Turbine speed.

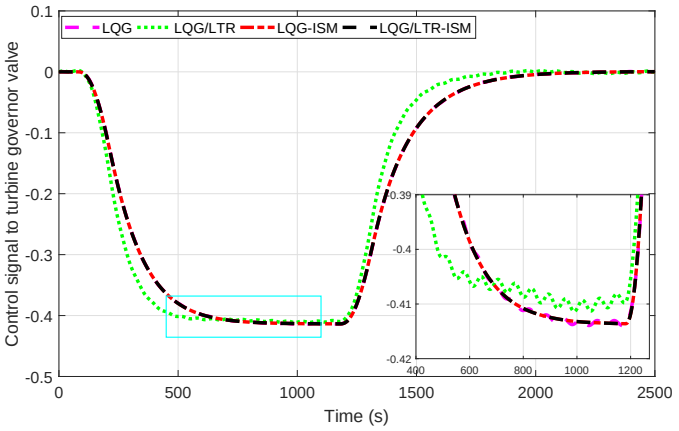

(c) Control signal to turbine governor valve.

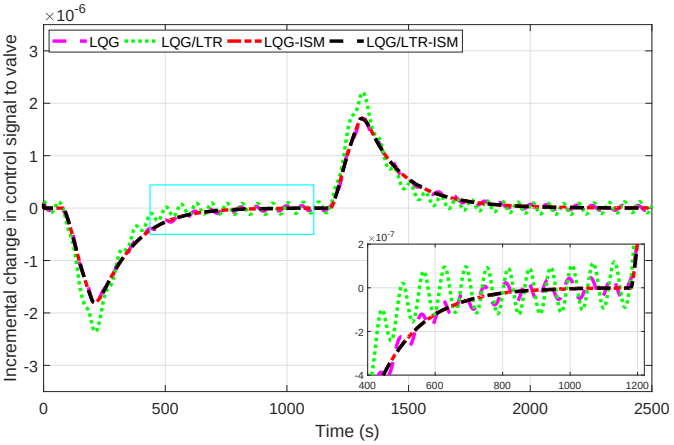

(d) Incremental change in control signal to valve.

Fig. 9: Variation of turbine-speed signals during a set-point change in demand power from the generator.

REFERENCES

[1] R. M. Edwards, K. Y. Lee, and M. A. Schultz, "State feedback assisted classical control: An incremental approach to control modernization of existing and future nuclear reactors and power plants," *Nuclear Technology*, vol. 92, no. 2, pp. 167–185, 1990.

[2] H. Arab-Alibeik and S. Setayeshi, "Improved temperature control of a PWR nuclear reactor using an LQG/LTR based controller," *IEEE Transactions on Nuclear Science*, vol. 50, pp. 211–218, 2003.

[3] G. Li and F. Zhao, "Flexibility control and simulation with multi-model and LQG/LTR design for PWR core load following operation," *Annals of Nuclear Energy*, vol. 56, pp. 179 – 188, 2013.

[4] G. Li, "Modeling and LQG/LTR control for power and axial power difference of load-follow PWR core," *Annals of Nuclear Energy*, vol. 68, pp. 193–203, 2014.

[5] J. Wan and P. Wang, "LQG/LTR controller design based on improved SFACC for the PWR reactor power control system," *Nuclear Science and Engineering*, vol. 194, no. 6, pp. 433–446, 2020.

[6] S. G. Chi and N. Z. Cho, "H∞ control theory applied to xenon control for load-following operation of a nuclear reactor," *Nuclear Technology*, vol. 137, no. 2, pp. 127–138, 2002.

[7] H. M. Emara, A. A. Hanafy, M. M. Z. Abdelaal, and S. Elaraby, "A novel, robust control methodology application to nuclear reactors," *Nuclear Science and Engineering*, vol. 174, no. 1, pp. 87–95, 2013.

[8] G. Li, B. Liang, X. Wang, and X. Li, "Multivariable modeling and nonlinear coordination control of nuclear reactor cores with/without xenon oscillation using H∞ loop shaping approach," *Annals of Nuclear Energy*, vol. 111, pp. 82–100, 2018.

[9] X. Yan, P. Wang, J. Qing, S. Wu, and F. Zhao, "Robust power control design for a small pressurized water reactor using an H infinity mixed sensitivity method," *Nuclear Engineering and Technology*, 2020.

[10] A. Etchepareborda and J. Lolich, "Research reactor power controller design using an output feedback nonlinear receding horizon control method," *Nuclear Engineering and Design*, vol. 237, no. 3, pp. 268–276, 2007.

[11] M. G. Na, I. J. Hwang, and Y. J. Lee, "Design of a fuzzy model predictive power controller for pressurized water reactors," *IEEE Transactions on Nuclear Science*, vol. 53, no. 3, pp. 1504–1514, 2006.

[12] H. Eliasi, M. B. Menhaj, and H. Davilu, "Robust nonlinear model predictive control for nuclear power plants in load following operations with bounded xenon oscillations," *Nuclear Engineering and Design*, vol. 241, pp. 533–543, 2011.

[13] G. Wang, J. Wu, B. Zeng, Z. Xu, W. Wu, and X. Ma, "Design of a model predictive control method for load tracking in nuclear power plants," *Progress in Nuclear Energy*, vol. 101, pp. 260–269, 2017.

[14] V. Vajpayee, S. Mukhopadhyay, and A. P. Tiwari, "Data-driven subspace predictive control of a nuclear reactor," *IEEE Transactions on Nuclear Science*, vol. 65, no. 2, pp. 666–679, Feb 2018.

[15] G. Ansarifar, H. A. Talebi, and H. Davilu, "Adaptive estimator-based dynamic sliding mode control for the water level of nuclear steam generators," *Progress in Nuclear Energy*, vol. 56, pp. 61 – 70, 2012.

[16] R. K. Munje, B. M. Patre, S. R. Shimjith, and A. P. Tiwari, "Sliding mode control for spatial stabilization of advanced heavy water reactor," *IEEE Transactions on Nuclear Science*, vol. 60, no. 4, pp. 3040–3050, 2013.

[17] G. R. Ansarifar, M. H. Esteki, and M. Arghand, "Sliding mode observer design for a pwr to estimate the xenon concentration & delayed neutrons precursor density based on the two point nuclear reactor model," *Progress in Nuclear Energy*, vol. 79, pp. 104 – 114, 2015.

[18] G. R. Ansarifar and M. Rafiei, "Second-order sliding-mode control for a pressurized water nuclear reactor considering xenon concentration feedback," *Nuclear Engineering and Technology*, vol. 36, pp. 94–101, 2015.

TABLE II: Performance comparison of different control approaches

Case	Technique	PRMSE	TVI	$\mathcal{L}_2NI$
A.1	LQG	1.149×10^{0}	2.780×10^{-2}	2.170×10^{0}
	LQG/LTR	2.470×10^{0}	2.440×10^{-2}	2.132×10^{0}
	LQG-ISM	9.245×10^{-1}	$\mathbf{2.320 \times 10^{-2}}$	2.138×10^{0}
	LQG/LTR-ISM	$\mathbf{9.242 \times 10^{-1}}$	2.322×10^{-2}	$\mathbf{2.129 \times 10^{0}}$
A.2	LQG	3.166×10^{0}	9.120×10^{-2}	5.378×10^{0}
	LQG/LTR	6.046×10^{0}	9.080×10^{-2}	5.105×10^{0}
	LQG-ISM	3.006×10^{0}	$\mathbf{9.054 \times 10^{-2}}$	4.911×10^{0}
	LQG/LTR-ISM	$\mathbf{3.004 \times 10^{0}}$	9.990×10^{-2}	$\mathbf{4.909 \times 10^{0}}$
B	LQG	1.281×10^{2}	2.931×10^{-2}	2.268×10^{0}
	LQG/LTR	1.285×10^{2}	3.750×10^{-2}	2.265×10^{0}
	LQG-ISM	1.276×10^{2}	$\mathbf{2.530 \times 10^{-2}}$	2.259×10^{0}
	LQG/LTR-ISM	$\mathbf{1.272 \times 10^{2}}$	2.531×10^{-2}	$\mathbf{2.258 \times 10^{0}}$
C	LQG	1.596×10^{-1}	8.740×10^{-2}	2.185×10^{1}
	LQG/LTR	1.687×10^{-1}	8.870×10^{-2}	2.161×10^{1}
	LQG-ISM	2.842×10^{-2}	$\mathbf{4.910 \times 10^{-2}}$	2.141×10^{1}
	LQG/LTR-ISM	$\mathbf{2.830 \times 10^{-2}}$	4.930×10^{-2}	$\mathbf{2.140 \times 10^{1}}$
D.1	LQG	2.483×10^{-1}	7.705×10^{2}	1.611×10^{5}
	LQG/LTR	2.483×10^{-1}	7.704×10^{2}	1.611×10^{5}
	LQG-ISM	2.481×10^{-1}	$\mathbf{7.681 \times 10^{2}}$	1.609×10^{5}
	LQG/LTR-ISM	$\mathbf{2.480 \times 10^{-1}}$	7.682×10^{2}	$\mathbf{1.608 \times 10^{5}}$
D.2	LQG	1.111×10^{-1}	5.991×10^{1}	7.209×10^{3}
	LQG/LTR	1.111×10^{-1}	5.991×10^{1}	7.208×10^{3}
	LQG-ISM	1.109×10^{-1}	$\mathbf{5.026 \times 10^{1}}$	7.208×10^{3}
	LQG/LTR-ISM	$\mathbf{1.108 \times 10^{-1}}$	5.027×10^{1}	$\mathbf{7.206 \times 10^{3}}$
D.3	LQG	3.915×10^{-1}	1.306×10^{1}	1.031×10^{3}
	LQG/LTR	3.915×10^{-1}	1.306×10^{1}	1.031×10^{3}
	LQG-ISM	3.741×10^{-1}	$\mathbf{5.890 \times 10^{0}}$	1.025×10^{3}
	LQG/LTR-ISM	$\mathbf{3.736 \times 10^{-1}}$	5.895×10^{0}	$\mathbf{1.023 \times 10^{3}}$
E	LQG	4.907×10^{0}	8.505×10^{-1}	4.062×10^{2}
	LQG/LTR	$\mathbf{3.979 \times 10^{0}}$	9.100×10^{-1}	4.097×10^{2}
	LQG-ISM	4.890×10^{0}	$\mathbf{8.275 \times 10^{-1}}$	4.061×10^{2}
	LQG/LTR-ISM	4.890×10^{0}	8.278×10^{-1}	$\mathbf{4.060 \times 10^{2}}$

[19] G. Ansarifar and H. Akhavan, "Sliding mode control design for a PWR nuclear reactor using sliding mode observer during load following operation," *Annals of Nuclear Energy*, vol. 75, pp. 611–619, 2015.

[20] P. V. Surjagade, A. P. Tiwari, and S. R. Shimjith, "Robust optimal integral sliding mode controller for total power control of large phwrs," *IEEE Transactions on Nuclear Science*, vol. 65, no. 7, pp. 1331–1344, 2018.

[21] P. V. Surjagade, S. Shimjith, and A. Tiwari, "Second order integral sliding mode observer and controller for a nuclear reactor," *Nuclear Engineering and Technology*, vol. 52, no. 3, pp. 552–559, 2020.

[22] R. J. Desai, B. M. Patre, R. K. Munje, A. P. Tiwari, and S. R. Shimjith, "Integral sliding mode for power distribution control of advanced heavy water reactor," *IEEE Transactions on Nuclear Science*, vol. 67, no. 6, pp. 1076–1085, 2020.

[23] M. N. Khajavi, M. B. Menhaj, and A. A. Suratgar, "A neural network controller for load following operation of nuclear reactors," *Annals of Nuclear Energy*, vol. 29, no. 6, pp. 751–760, 2002.

[24] S. S. Khorramabadi, M. Boroushaki, and C. Lucas, "Emotional learning based intelligent controller for a PWR nuclear reactor core during load following operation," *Annals of Nuclear Energy*, vol. 35, no. 11, pp. 2051–2058, 2008.

[25] G. Wang, J. Wu, B. Zeng, Z. Xu, and X. Ma, "A nonlinear adaptive sliding mode control strategy for modular high-temperature gas-cooled reactors," *Progress in Nuclear Energy*, vol. 113, pp. 53 – 61, 2019.

[26] S. M. H. Mousakazemi, N. Ayoobian, and G. R. Ansarifar, "Control of the reactor core power in PWR using optimized PID controller with the real-coded GA," *Annals of Nuclear Energy*, vol. 118, pp. 107–121, 2018.

[27] V. Utkin and J. Shi, "Integral sliding mode in systems operating under uncertainty conditions," in *Proceedings of 35th IEEE Conference on Decision and Control*, vol. 4, Dec 1996, pp. 4591–4596 vol.4.

[28] R. M. Edwards, K. Y. Lee, and A. Ray, "Robust optimal control of nuclear reactors and power plants," *Nuclear Technology*, vol. 98, no. 2, pp. 137–148, 1992.

[29] R. Shaffer, W. He, and R. M. Edwards, "Design and validation of optimized feedforward with robust feedback control of a nuclear reactor," *Nuclear Technology*, vol. 147, no. 2, pp. 240–257, 2004.

[30] G. Ablay, "A modeling and control approach to advanced nuclear power plants with gas turbines," *Energy Conversion and Management*, vol. 76, pp. 899–909, 2013.

[31] Z. Dong, Y. Pan, Z. Zhang, Y. Dong, and X. Huang, "Model-free adaptive control law for nuclear superheated-steam supply systems," *Energy*, vol. 135, pp. 53–67, 2017.

[32] V. Vajpayee, V. Becerra, N. Bausch, J. Deng, S. R. Shimjith, and A. J. Arul, "Dynamic modelling, simulation, and control design of a pressurized water-type nuclear power plant," *Nuclear Engineering and Design*, vol. 370, p. 110901, 2020.

[33] C. S. Subudhi, T. U. Bhatt, and A. P. Tiwari, "A mathematical model for total power control loop of large PHWRs," *IEEE Transactions on Nuclear Science*, vol. 63, no. 3, pp. 1901–1911, June 2016.

[34] T. W. Kerlin, *Dynamic Analysis and Control of Pressurized Water Reactors*. Academic Press, 1978, vol. 14.

[35] M. R. A. Ali, *Lumped Parameter, State Variable Dynamic Models for U-tube Recirculation Type Nuclear Steam Generators*. PhD dissertation, University of Tennessee, Knoxville, 1976.

[36] M. Naghedolfeizi, *Dynamic Modeling of a Pressurized Water Reactor Plant for Diagnostics and Control*. Master's thesis, University of Tennessee, Knoxville, 1990.

[37] L. Wang, W. Sun, J. Zhao, and D. Liu, "A speed-governing system model with over-frequency protection for nuclear power generating units," *Energies*, vol. 13, no. 173, 2020.

[38] D. S. Naidu, *Optimal control systems*. CRC press, 2002.

[39] J. Doyle and G. Stein, "Multivariable feedback design: Concepts for a classical/modern synthesis," *IEEE Transactions on Automatic Control*, vol. 26, no. 1, pp. 4–16, 1981.

[40] M. T. Hamayun, C. Edwards, and H. Alwi, *Fault tolerant control using integral sliding modes*. Springer, Cham, 2016.

[41] C. Edwards and S. K. Spurgeon, *Sliding Mode Control: Theory and Applications*. Taylor and Francis, 1998.

[42] *Westinghouse Technology Course R-104P Manual*. US-NRC Technical Training Center, 2012. [Online]. Available: https://www.nrc.gov/docs/ML0230/

[43] A. H. Harvey, *Thermodynamic Properties of Water: Tabulation from the IAPWS Formulation 1995 for the Thermodynamic Properties of Ordinary Water Substance for General and Scientific Use*. NISTIR, 1998. [Online]. Available: https://www.nist.gov/srd/nistir-5078

TABLE A.1: Typical Parameters of a Westinghouse-type 1.2 GWe PWR Plant

$\lambda_1(s^{-1})$ 1.2437×10^{-2}	$\lambda_2(s^{-1})$ 3.05×10^{-2}	$\lambda_3(s^{-1})$ 1.1141×10^{-1}	$\lambda_4(s^{-1})$ 3.013×10^{-1}	$\lambda_5(s^{-1})$ 1.12866	$\lambda_6(s^{-1})$ 3.0130
β_1 2.15×10^{-4}	β_2 1.424×10^{-3}	β_3 1.274×10^{-3}	β_4 2.568×10^{-3}	β_5 7.48×10^{-4}	β_6 2.73×10^{-4}
$\Lambda(s)$ 3×10^{-5}	$H_f(^0Cs^{-1})$ 71.8725	$H_c(^0Cs^{-1})$ 1.1254	$\tau_f(s)$ 4.376	$\tau_c(s)$ 10.893	$\tau_r(s)$ 0.703
$\tau_{rxu}(s)$ 2.517	$\tau_{rxi}(s)$ 2.145	$\tau_{hot}(s)$ 0.234	$\tau_{cold}(s)$ 1.310	$\tau_{sgu}(s)$ 0.726	$\tau_{sgi}(s)$ 0.659
$\tau_{p1}(s)$ 1.2815	$\tau_{p2}(s)$ 1.2815	$\tau_{pm1}(s)$ 0.5826	$\tau_{pm2}(s)$ 0.5826	$\tau_{mp1}(s)$ 0.3519	$\tau_{mp2}(s)$ 0.1676
$\tau_{ms1}(s)$ 0.3519	$\tau_{ms2}(s)$ 0.1676	$U_{ms1}S_{ms1}(W^0C^{-1})$ 1.7295×10^8	$U_{ms2}S_{ms2}(W^0C^{-1})$ 3.6312×10^8	$c_{pfw}(J/kg.^0C)$ 5.4791×10^3	C_{tg} 2.0481
$\frac{\partial T_{sat}}{\partial p_s}(^0C/MPa)$ 9.47	$h_{ss}(J/kg)$ 2.7656×10^6	$K_s(J/MPa)$ 8.1016×10^7	$m_s(kg)$ 2.0518×10^3	$m_w(kg)$ 1.8167×10^4	$d_w(kg/m^3)$ 595.6684
$d_s(kg/m^3)$ 100.9506	$V_w(m^3)$ 30.4988	$A_p(m^2)$ 3.566	$l(m)$ 14.2524	$G(\Delta K/K)$ 14.5×10^{-3}	$\dot{m}_{sor}(kg/s)$ 2.1642×10^3
$h_{spr}(J/kg)$ 1.336×10^6	$h_w(J/kg)$ 1.6266×10^6	$h_{\bar{w}}(J/kg)$ 9.7209×10^5	$\nu_w(m^3/kg)$ 1.7×10^{-3}	$\nu_s(m^3/kg)$ 9.9×10^{-3}	J_p 5.4027
$V_1\vartheta_1(kg/^0C)$ 0.5991	$V_2\vartheta_2(kg/^0C)$ 0.1814	$V_3\vartheta_3(kg/^0C)$ 0.1814	$V_4\vartheta_4(kg/^0C)$ 1.3164	$V_5\vartheta_5(kg/^0C)$ 0.2752	$V_6\vartheta_6(kg/^0C)$ 2.776
$V_7\vartheta_7$ $(kg/^0C)$ 0.6022	$V_8\vartheta_8(kg/^0C)$ 0.6022	$V_9\vartheta_9(kg/^0C)$ 0.2776	$V_{10}\vartheta_{10}(kg/^0C)$ 0.1927	$K_{1p}(kg/kg.MPa)$ -8.152×10^{-3}	$K_{2p}(kg/m^3.MPa)$ 4.708×10^{-3}
$K_{3p}(J/m^3.MPa)$ -1.118×10^{-4}	$K_{4p}(m^3/kg.MPa)$ 4.708×10^{-3}	F_{hp} 0.33	F_{ip} 0	F_{lp} 0.67	O_{rv} 1.0
$\tau_{hp}(s)$ 10.0	$\tau_{ip}(s)$ 0.4	$\tau_{lp}(s)$ 1.0	κ_{hp} 0.8	J_{tur} 5.4040	$I_{tg}(kg.m^2)$ 1.99642×10^5
$\alpha_f(\Delta K/K/^0C)$ -2.16×10^{-5}	$\alpha_c(\Delta K/K/^0C)$ -1.8×10^{-4}	$\alpha_p(\Delta K/K/MPa)$ 1.5664×10^{-4}	$\tau_1(s)$ 5×10^{-8}	$\tau_2(s)$ 2×10^{-3}	$K_{lo}(mA)$ 1.9569
κ_{lo} 1.1067×10^{10}	$\tau_{rtd}(s)$ 8.2	$K_{rtd}(mA)$ 10.667	$K_{tg}(mA^{-1})$ 6.25	ζ_{tg} 0.4933	$\varpi_{tg}(rad/s)$ 14.6253
$P(GWe)$ 1.2	$T_{f0}(^0C)$ 626.66	$T_{c10}(^0C)$ 312.13	$T_{c20}(^0C)$ 327.30	$T_{rxu0}(^0C)$ 327.30	$T_{hot0}(^0C)$ 327.30
$T_{sgi0}(^0C)$ 327.30	$T_{sgu0}(^0C)$ 296.96	$T_{cold0}(^0C)$ 296.96	$T_{rxi0}(^0C)$ 296.96	$T_{p10}(^0C)$ 306.75	$T_{p20}(^0C)$ 296.96
$T_{m10}(^0C)$ 297.41	$T_{m20}(^0C)$ 292.51	$T_{s0}(^0C)$ 288.06	$p_{s0}(MPa)$ 7.28	$p_{p0}(MPa)$ 15.41	$l_{w0}(m)$ 28.06
$T_{rtd10}(^0C)$ 327.30	$T_{rtd20}(^0C)$ 327.30	$T_{fw}(^0C)$ 232.20	$i_{lo0}(mA)$ 19.65	$i_{rtd0}(mA)$ 14.66	$\omega_{tur0}(rad/s)$ 360